RSC Advances

PAPER

View Article Online
View Journal | View Issue

Cite this: *RSC Adv.*, 2026, **16**, 4723

Removal of the ionophore antibiotic narasin using vegetal materials as bioadsorbents

Samiha Hamdi,[abc] Manel Issaoui,[cd] Ainoa Míguez-González,[b] Raquel Cela-Dablanca,[b] Sonia Hammami,[c] Ana Barreiro,[*b] María J. Fernández-Sanjurjo,[b] Esperanza Álvarez-Rodríguez[b] and Avelino Núñez-Delgado[b]

The occurrence of ionophore antibiotics, particularly narasin (NAR), in the environment, has recently become a matter of concern because of their widespread use, high eco-toxicity, and environmental persistence. This study assessed the adsorption–desorption characteristics of NAR onto a variety of low-cost by-products using batch-type experiments. Fourier transform infrared (FTIR) spectroscopy was performed on all samples, whereas solid-state ^{13}C CP/MAS NMR analyses were undertaken on the six most effective adsorbents as well as on the three least efficient ones. The results show that, at low concentrations of antibiotic added (5–10 μmol L^{-1}), adsorption remained low, not exceeding 25.33%. At the three lowest concentrations (5–20 μmol L^{-1}), alfa, palm, and cactus fibers, as well as calcined coffee grounds exhibited adsorption rates always ≥65.12%. At concentrations ≥20 μmol L^{-1}, adsorption increased in bioadsorbents with higher organic matter content, reaching up to 100% for eucalyptus bark at 100 μmol L^{-1}. Adsorption data were adjusted to different models, with Freundlich presenting the best fit. No desorption was observed at low concentrations for most bioadsorbents, except for cactus and Mediterranean tapeweed fibers, as well as for raw and calcined coffee grounds, while it increased with higher concentrations (above 20 μmol L^{-1}), but generally remained below 10%, except for calcined coffee grounds and cactus fiber, where it reached 10.48% and 14.64%, respectively, at 100 μmol L^{-1} of NAR added. All these results indicate that NAR is strongly retained on the tested bioadsorbents, suggesting that the ecological risks associated with this pollutant can be mitigated using these bioadsorbents.

Received 1st December 2025
Accepted 16th January 2026

DOI: 10.1039/d5ra09276k

rsc.li/rsc-advances

1 Introduction

Antibiotics are vital in veterinary medicine and agriculture for treating infections and boosting productivity.[1,2] However, their overuse has led to widespread environmental contamination, with residues commonly detected in ecosystems.[3] Ionophore antibiotics (IPAs), including monensin (MON), salinomycin (SAL), lasalocid (LAS), and narasin (NAR), have been strictly used in veterinary medicine as coccidiostats for broilers and as growth promoters for ruminants like beef cattle.[4,5] Because of their higher toxicity compared to the non-ionophore antibiotics,[6] the widespread use of ionophores is considered as a pressing environmental and health concern. This is mainly attributable to their potential to disrupt ecosystems and foster antimicrobial resistance in soil bacterial communities, which can be transferred to humans *via* the food chain.[7,8]

Following administration in livestock feed, IPAs are poorly absorbed and predominantly excreted in animals' urine and feces,[9] thereby entering soils through the application of manure/slurry as fertilizers.[10] Although IPAs are hydrophobic compounds, once in soils, substantial concentrations can be transported with rainfall runoff from manure/sludge-fertilized fields,[11,12] reaching water bodies at levels up to 0.22 μg L^{-1},[11] while dropping to 0.031 μg L^{-1} in irrigation conveyances.[13]

Within this antibiotic group, NAR is a monocarboxylic polyether produced by *Streptomyces aureofacien*. Its unique molecular structure (Fig. S1, SI[14]) endows it remarkable chemical stability and a broad spectrum against most Gram (+) bacteria, anaerobic bacteria, and fungi.[15] This ionophore antibiotic is widely used as a coccidiostat feed additive in nearly all broiler chicken production.[16] Bearing in mind that NAR is unapproved for human therapeutic use due to its high toxicity, the potential detection of its residues in consumable food products from treated animal species or non-target species

[a]*Department of Biotechnology, Faculty of Science and Technology of Sidi Bouzid, University of Kairouan, 9100 Sidi Bouzid, Tunisia*

[b]*Department Soil Science and Agricultural Chemistry, Engineering Polytechnic School, University of Santiago de Compostela, 27002 Lugo, Spain. E-mail: ana.barreiro.bujan@usc.es*

[c]*Laboratory of Nutrition – Functional Foods and Health (NAFS)-LR12ES05, Faculty of Medicine, University of Monastir, Avenue Avicenne, 5019 Monastir, Tunisia*

[d]*Higher Institute of Applied Studies in Humanities of Sbeitla, University of Kairouan, Kasserine, Tunisia*

exposed to cross-contaminated feed can lead to human exposure and heighten associated public health concerns.[9]

From an environmental perspective, the presence of this anticoccidial in manure, water, and sediments, even at low concentrations, could pose several ecological risks.[10,17] Markedly, Barreiro *et al.* (2024)[18] found detectable levels of NAR in 21% of the 66 samples analyzed of manure and slurry. Furtula *et al.* (2010)[19] further reported a worst-case NAR concentration in poultry litter, 12.7 mg kg^{-1} d. w.

Interestingly, the occurrence of NAR has been reported to adversely affect the biogeochemical nitrogen cycle in cultivated sandy loam soil following manure application. Documented effects include increased NH_4^+ levels in field moist soils, reduced nitrate concentrations, and overall soil nitrogen depletion resulting from increased N_2O flux in response to trace NAR exposure.[20] Furthermore, NAR residues in soil (at 6–10 mg kg^{-1} d. w.) have been shown to accumulate in edible crops like carrots, thereby entering the food chain.[21] Other authors have outlined the impacts of NAR present in water on aquatic life; among them, Kim and Carlson (2006)[17] estimated the risk related to NAR residues accumulated in sediments on stream benthic biota.

Because of the inefficiency of conventional treatment methods, NAR has been found in effluents and sludge from WWTPs,[22] as well as in surface waters downstream of WWTP discharge points, where it was quantified in 8% of the samples, with mean concentrations of 9.3 ng L^{-1}.[23]

Despite the existing background, studies on the environmental repercussions and cost-effective removal of NAR, particularly from water, remain scarce. Most existing research focuses on its sorption in soils under varying conditions,[24] underscoring the urgent need for advanced adsorption-based remediation strategies.

In recent decades, the use of cost-efficient and eco-friendly bioadsorbents has emerged as a valuable approach that aids in recycling waste by-products while retaining emerging contaminants, which is of clear importance in terms of preserving environmental and public health.[25] However, despite the research advancements in this field, the specific capacity of a variety of biomaterials to adsorb ionophore antibiotics like NAR from water or soils has yet to be investigated. For instance, in Tunisia, the forestry, agro-food, and marine sectors generate significant annual quantities of residues that remain largely unexploited, despite governmental efforts,[26] rendering their valorization in the remediation of emerging pollutants like NAR of great relevance.

Taking this background into account, and serving as initial steps within a broader research program,[27] the present research was designed with the objective of addressing the NAR removal from an artificially contaminated aqueous solutions under experimental conditions, using fourteen porous bioadsorbents (seven natural fibers and barks, as well as seven agro-food by-products), characterized by different physicochemical properties and collected from various Tunisian regions. To our knowledge, data concerning the adsorption of ionophore antibiotics such as NAR, using low-cost bioadsorbents through batch-type experiments were scarce. Therefore, research addressing this topic would be clearly relevant to shed further light on adsorption mechanism affecting to NAR onto these biomaterials. The findings of this research could address two key challenges: (i) from an economic standpoint, they may support the appropriate use of the studied by-products as value-added materials, promoting their effective recycling; and (ii) from an ecological front, they could help mitigate the risks associated with the release of NAR residues into the environment, thereby safeguarding both human and environmental health.

2 Experimental

2.1 Bioadsorbent by-products

For this research, fourteen by-products of forestry and agro-food origin were investigated, as presented in Table S1 (SI). Six of these, encompassing natural fibers (alfa, AF; cactus, CF; and palm, PF) and barks (acacia, AB; eucalyptus, EB; zean oak, ZOB), were previously described in Hamdi *et al.* (2024).[28] The other seven bioadsorbents used were agro-food by-products consisting of orange (OP) and pomegranate (PGP) peels, almond (AS) and pea (PS) shells, date palm stones (DPS), and coffee grounds, both raw (CGs) and calcined (CC). Additionally, mediterranean tapeweed (*Posidonia oceanica*) fiber (POF) was tested as well.

All collected samples were rinsed repeatedly with distilled water, oven-dried at 60 °C for 24 h, ground using an automatic mill (SCP SCIENCE SP-2000 Swing Mill Grinder, USA), and sieved through a 100 μm mesh to ensure uniform particle size (≥100 μm). Finally, the powders were stored under laboratory conditions (25 ± 2 °C) until further analysis. Further sampling and methodological details are described in Hamdi *et al.* (2024).[28]

2.2 Chemicals and reagents

For this research, the ionophore antibiotic NAR was supplied as PX-Narasin, 35 g kg^{-1}, a commercially available mixture intended for being added to animal feed/treatment, with its basic physicochemical characteristics summarized in Table S2 (SI).

Moreover, high-purity compounds, such as methanol, acetic acid, trichloroacetic (TCA), and 2,4-dinitrophenol (DNP), were purchased from Sigma-Aldrich (Madrid, Spain).

The stock solution of the antibiotic was initially prepared at 5 mmol L^{-1} in 96% methanol (Panreac, Madrid, Spain), then diluted with Milli-Q water (Millipore, Madrid, Spain) to obtain a 100 μmol L^{-1} solution and stored in the dark at −18 °C. To perform HPLC analysis, all the NAR aqueous solutions with of different concentrations were prepared from this stock by successive dilution with Milli-Q water (Millipore, Madrid, Spain) containing 0.005 mol L^{-1} $CaCl_2$ as electrolyte.

2.3 Adsorption and desorption experiments

Batch-type experiments were performed to study the adsorption/desorption of NAR on/from the different bioadsorbents. To achieve this, 0.5 g of each sample was weighed, then adding 10 mL of a solution with different concentrations of the antibiotic (5, 10, 20, 40, 80, and 100 μmol L^{-1}), also

containing 0.005 mol L^{-1} $CaCl_2$ as background electrolyte. The suspensions were stirred in the dark for 48 h using a rotary shaker (SIR EM-SA, motor: 220 V, N_1: 2700 rpm, N_2: 48 rpm), at 50 rpm. Afterward, these suspensions were centrifuged at 4000 rpm for 15 min and the resulting supernatants were subsequently filtered through 0.45 μm nylon syringe filters (Fisher Scientific, Madrid, Spain). Ultimately, the antibiotic concentrations in the equilibrium solution were measured by means of HPLC-UV with an LPG 3400 SD equipment (Thermo Fisher, Waltham, MA, USA), following derivatization of each prepared sample. Additional details regarding the derivatization method, quantification procedure, and the HPLC equipment employed for these analyses, are presented in SI. Furthermore, examples of HPLC curves obtained are illustrated in Fig. S2 (SI).

It is essential to emphasize that the contact time, adsorbent dosage, and antibiotic concentrations are selected on the basis of previous studies addressing the adsorption of comparable ionophores, such as monensin and salinomycin, onto forest by-products and clays.[28,29] The assays were conducted in the dark to prevent NAR photodegradation, while the experimental setup was designed to mimic environmentally relevant conditions, being carried out at room temperature (25 ± 2 °C) and under unmodified (natural) pH conditions.

In the case of the samples used for the adsorption studies as a function of pH, the experiment was carried out at pH between 2 and 10, adjusting with different volumes of 0.5 mol L^{-1} HCl and 0.5 mol L^{-1} NaOH, using only the highest initial concentration of NAR, 100 μmol L^{-1}.

Regarding the desorption, experiments were carried out by adding 10 mL of a 0.005 mol L^{-1} $CaCl_2$ solution to the material remaining from the adsorption tests and previously weighted. The samples were then agitated for 48 h, followed by centrifugation, filtration, and derivatization under the same conditions as in the adsorption step. Furthermore, reusability was evaluated through six consecutive adsorption–desorption cycles, using 0.1 mol L^{-1} HCl for desorption and 0.1 mol L^{-1} NaOH for neutralization.[30] The regenerated sorbent was filtered, repeatedly washed, and then reused following the same protocol as adsorption.

Lastly, the NAR concentrations in the equilibrium solutions were quantified using the same method applied during the adsorption phase. All measurements and adsorption–desorption experiments were performed in triplicate ($n = 3$), with error bars corresponding to the standard deviation.

2.4 ^{13}C CP/MAS NMR spectroscopy

Solid-state ^{13}C CP/MAS NMR spectra were acquired using a Bruker INOVA-400 NMR spectrometer for five out of the fourteen studied by-products, selected for their stronger capacity to retain NAR in aqueous solutions (with slower desorption), as well as for three by-products showing the lowest sorption efficacy, according to the adsorption–desorption results. Spectra were divided into four different spectral regions: alkyl C (0–45 ppm), *O*-alkyl C (45–110 ppm), aromatic-C (110–160 ppm), and carboxyl-C (160–220 ppm). Total and relative signal intensities of each functional group were determined by integrating over the spectral areas with the calculation routine of the spectrometer.

2.5 Fourier-transform infrared (FIIR) spectroscopy

In this study, Fourier-transform infrared (FTIR) analyses of the bioadsorbents under investigation, both before (raw materials) and after adsorption (with 100 μmol L^{-1} of NAR), were performed using a FTIR-Bomen MB102 instrument (ABB, Switzerland), allowing to elucidate the interactions between the studied antibiotic and the bioadsorbent surfaces. All the IR spectra were acquired through transmittance measurements using KBr pellets, covering the spectral range from 400 to 4000 cm^{-1}, with a resolution of 4 cm^{-1}.

2.6 Statistical analysis and data treatment

Data from the adsorption tests were fitted to three different models: Freundlich, Langmuir, and Linear. Following desorption determinations, the hysteresis index (HI) was calculated. More details are indicated in SI.

Additionally, the Scatchard model was applied by plotting q_a/C_{eq} *versus* q_a (C_{eq}: equilibrium concentration, μmol L^{-1}; q_a: adsorbed amounts of NAR, μmol kg^{-1}), with the obtained plots interpreted as previously indicated by Hamdi *et al.* (2024).[28]

The SPSS Statistics 21 software was used to adjust the experimental adsorption data to the three selected models, as well as to perform bivariate Pearson's correlations between adsorption–desorption data (the latter using percentage values observed at 100 μmol L^{-1} of NAR)/the K_F and n values resulted from the Freundlich equation, and the main characteristics of the bioadsorbents.

3 Results and discussion

3.1 Characteristics of the adsorbents

The main physicochemical properties of all the bioadsorbents under study are presented in Table S3 (SI), with corresponding details also provided in the SI. Elemental composition of the bioadsorbents is likewise presented in Table 1. Briefly, carbon content was found to range from 15.1% for CC to 48.3% for AB, which is typical for this type of biomass and in agreement with values reported in the literature for agro-forest wastes, such as orange peel and eucalyptus bark[31,32] (Table 1). Oxygen, nitrogen, and hydrogen contents also exhibited wide variability among the samples, ranging from 6.13–48.7%, 0.02–44.21%, and 0.45–7.3%, respectively, with the highest values being recorded for PS, OP, and DPS. Results evidenced the presence of sulfur and chloride in certain samples and their absence in others; nevertheless, in all cases they remained minor constituents, with values not exceeding 0.5% (for PF) and 0.36% (EB), respectively.

Furthermore, several studies on the physical properties of agro-forest by-products have revealed that it contains cellulose, hemicellulose, lignin, and pectin.[33,34] In this study, it was found that, as expected, holocellulose (cellulose and hemicelluloses) constitutes the major component of all the analyzed samples

Table 1 Contents of main chemical constituents of the adsorbent biomaterials[a]

Chemical composition	By-products/mass (%)													
	AF	CF	PF	POF	AB	EB	ZOB	OP	PGP	PS	As	DPS	CGs	CC
Carbon	42.3	33.4	42.8	46.5	48.3	47.5	45.3	47.20	29.36	44.0	70.3	41.41	35.3	15.1
Oxygen	47.3	—	—	41.4	46.3	45.1	43.5	6.13	47.21	48.7	21.9	—	33.2	8.3
Nitrogen	0.03	1.3	0.8	0.02	0.26	0.31	0.19	44.21	0.67	1.81	3.4	1.56	2.4	0.21
Hydrogen	6.3	—	4.6	5.3	5.2	4.9	4.1	1.4	4.67	5.6	—	7.3	6.7	0.45
Sulfur	—	—	0.5	0.342	0.06	0.01	0.05	0.06	0.09	—	—	0.32	0.2	0.01
Chloride	—	—	—	—	0.24	0.36	0.33	0.01	—	—	—	—	—	—
Cellulose	48.1	52.4	42.9	46.8	45.7	44.3	30.6	31.2	29.4	35.4	43.2	33.8	15.7	1.22
Hemicellulose	29.0	9.1	16.3	21.3	18.8	19.22	22.4	17.01	13.6	26.3	19.3	25.6	35.6	—
Holocellulose (cellulose + hemicellulose)	75.1	61.5	59.2	68.1	64.5	63.52	53.0	48.01	43.0	61.7	62.5	59.4	51.3	1.22
Lignin	12.3	11.3	32.1	32.6	14.1	22.46	18.9	20.5	21.4	18.3	28.0	31.2	3.5	0.3
Pectin	2.3	13.4	3.6	—	1.3	1.02	15.2	3.39	10.9	7.8	1.0	3.4	0.9	—
Water-soluble compounds	10.3	13.8	5.1	3.7	16.5	13.0	12.9	27.9	24.7	12.2	7.3	6.0	28.0	1.7

[a] —: not detected.

(between 43.0–77.1%, except for CC, 1.22%), with the maximum proportion observed in AF (Table 1). These results are similar to those previously reported by Ncibi *et al.* (2009)[35] and Khiari *et al.* (2010)[36] for *Posidonia* fiber, and by Ayadi *et al.* (2023)[37] for alfa fiber.

According to Table 1, most of the adsorbent by-products contain a relatively high amount of lignin (ranging from 11.3% to 32.6%), except for CC (0.3%) due to degradation during calcination, compared to typical amounts found in non-wood annual plants.[38] The highest lignin contents were found in PF and POF fibers (32.1% and 32.6%, respectively), followed by ZOB, AS, and DPS samples (28.0–31.2%) (Table 1). Conversely, pectin constitutes a minor component in these materials, ranging from 0.0% for POF to 15.2% for OP, and was markedly lower than the values reported by Fakayode and Abobi (2018)[39] for orange peel, likely reflecting the impact of oven-heating in this study.

In addition to that, Fig. S3 (SI) displays the relative contents of surface functional groups of the studied bioadsorbents, with analysis conducted for the present study.

Generally, the principal surface functional groups are carboxylic acids, phenol, and carbonyl, with Fig. S3 (SI) proving that the concentration of the acidic functions is more important than basic ones on the surface of the biosorbent (oscillating between 1.1 meq g^{-1} for CF and 3.5 meq g^{-1} for PGP). In this regard, Ben-Ali *et al.* (2021)[40] reported comparable values for Tunisian pomegranate peel as found here.

3.2 Adsorption capacity

Fig. 1 illustrates the NAR adsorption (calculated in μmol kg^{-1}) as a function of the initially added concentrations of the antibiotic (μmol L^{-1}), whereas Fig. S4 (SI) presents the adsorption results expressed as a percentage.

Considering Fig. 1, the adsorption results indicate that for the highest NAR concentration added (100 μmol L^{-1}), both AB and EB showed the biggest values, 1927.64 and 1956.98 μmol kg^{-1}, respectively. These scores represent 98.51% and 100%, respectively of the added NAR (Fig. S4). Regarding the fiber bioadsorbents, NAR adsorption differed among them, with AF adsorbing similar concentrations compared to the two latter barks (1919.12 μmol kg^{-1}, 97.98% at 100 μmol L^{-1} of NAR added). Meanwhile, the adsorption of the other fibers was smaller (CF < PF < POF (*Posidonia oceanica* fiber)) for the highest NAR concentration added, not surpassing 77.40% in any case (meaning 1548.0 μmol kg^{-1}).

On the other hand, at the lower concentrations of added NAR (5 and 10 μmol L^{-1}), the adsorption percentages were higher for AF, CF, and PF (between 65.12% and 83.34%).In contrast, the bark samples and POF exhibited a retention capacity of less than 26% at these concentrations of NAR (Fig. S4).

Among the agro-food bioadsorbents, almond shell (AS), orange peel (OP), and date palm stones (DPS) were the ones showing greater adsorption capacity under the three highest added doses of NAR (Fig. 1 and S4), with retained amounts of approximately 1873.21 μmol kg^{-1} (93.44%), 1853.46 μmol kg^{-1} (92.65%), and 1834.53 μmol kg^{-1} (91.72%), respectively. Conversely, calcined coffee grounds adsorbed better (between 79.78% and 90%) (Fig. 1 and S4) at the three lowest antibiotic concentrations (5–20 μmol L^{-1}).

The BET method, applied to determine the specific surface area (S_{BET}), together with the pore volumes (PV) and pore sizes (PS), revealed higher S_{BET} and PV values for the samples retaining more NAR molecules at 100 μmol L^{-1} (AF, AB, EB, OP, AS, and DPS) compared to all the remaining samples (except for PF). These values oscillated between 0.468–2.683 m^2 g^{-1} and 0.031–0.083 cm^3 g^{-1}, respectively (Table S3, SI). Meanwhile, they presented moderate PS values, ranging from 8.22 to 12.67 nm (Table S3, SI).The S_{BET} values justifies the stronger sorption capacity observed for the aforementioned adsorbents at 100 μmol L^{-1} of pollutant, whereas the values PS confirmed their mesoporous nature based on the IUPAC nomenclature of porous materials (microporous: <2 nm; mesoporous: 2–50 nm; and macro-porous: >50 nm).[41]

With respect to the two smallest added concentrations of NAR (5–10 μmol L^{-1}), adsorption percentages ranged from 0% to 25.33% for most of the bioadsorbents (except for AF, CF, PF,

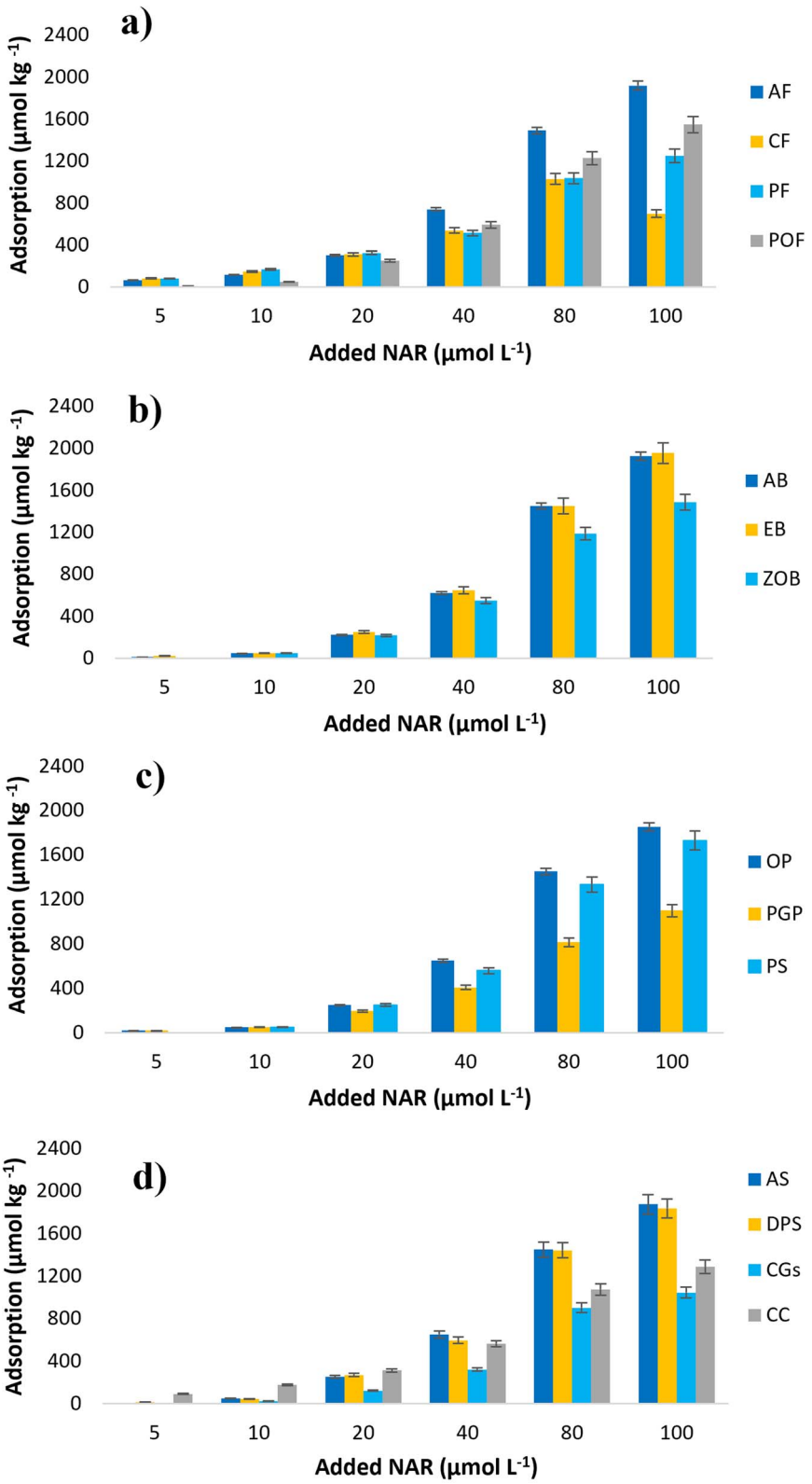

Fig. 1 Adsorption curves of narasin (NAR) (expressed in µmol kg^{-1} and as %) for the natural fibers (a), barks (b), and the agro-food by-products (c and d), as a function of the antibiotic concentration added (µmol L^{-1}). Average values ($n = 3$), with coefficients of variation always <5%, and error bars represent the standard deviation.

and CC). By contrast, at higher concentrations (40–100 μmol L^{-1}), they generally increased for all products (oscillating between 52.8% for coffee grounds (CGs) and 100% for eucalyptus bark), except for CF and PF, as well as the CC sample, whose adsorption dropped to 34.92, 62.51, and 64.78%, respectively, at 100 μmol L^{-1} of NAR (Fig. S4). This can be explained by the fact that the adsorption percentages tend to increase as more molecules become available.[42]

The bioadsorbents CF and PF, and CC displayed substantial NAR adsorption rates at the three lowest concentrations added (5–20 μmol L^{-1}), with retention rates of 69.58–90%, closely approaching their performance at higher concentrations (between 40–100 μmol L^{-1}) (ranging 62.51–70.34%; except for CF, which dropped to 34.92% at 100 μmol L^{-1}), which makes them more effective than CF for adsorbing this antibiotic regardless of the concentration added.

It is worth noting that POF, ZOB, and PS presented adsorption scores at NAR concentrations between 40 and 100 μmol L^{-1} within the range of 69.8% to 86.53%, which were slightly higher than those recorded for the aforementioned bioadsorbents, namely PF and CC.

Comparatively, the CGs stood out as the bioadsorbent with the weakest adsorption capacity at the two smallest concentrations, 5 and 10 μmol L^{-1}, with corresponding scores of 0% and 10.67%, respectively.

Analyzing adsorption as a function of NAR concentration may not provide a clear comparative overview of adsorbent performance. In this context, mean adsorption values offer a more suitable basis for comparison. Fig. S5 (SI) shows that CGs exhibited the lowest mean adsorption (30.3%), whereas AF recorded the highest (78.7%). Overall, the adsorption means across the tested bioadsorbents followed the sequence: CGs < PGP < AB < ZOB < POF < PS < AS < DPS < OP < EB < CF < PF < CC < AF (Fig. S5).

These noteworthy differences in adsorption performance against NAR among the bioadsorbents may be attributable to their clearly different physicochemical characteristics, especially pH (Table S3, SI). Hence, a bivariate correlation analysis was conducted to critically assess the relationship between adsorption data and bioadsorbent properties, revealing a significant negative correlation between adsorption percentages (recorded at 100 μmol L^{-1} of NAR) with pH_{KCl} values ($r = -0.717$ and $p < 0.01$). However, no significant correlation was observed with pH in water (pH_w) ($r = -0.371$) (Table S4, SI).

Nevertheless, it is evident to note that the bioadsorbents showing higher adsorption scores at the highest NAR concentrations were mostly those having pH_w values ranging from 4.5 to 5.4 (AF, AB, EB, AS, OP, and DPS). The last trend also applies when observing the equilibrium pH values (pH_{eq}) (Table S5, SI).

Other researchers have reported the inverse effect of pH on NAR adsorption in soils,[24] which is also in line with the trends reported elsewhere on monensin and lasalocid.[43] In general, in environmental studies, surrounding pH is considered as one of the most influential parameters affecting antibiotic–biosorbent interactions, as it concurrently affects the chemical speciation of the pollutants and adsorbent surfaces.[44] Thus, comparing adsorption data for each by-product with pH_{eq} (expressed as mean values) could offer valuable insights into the underlying adsorption process; however, in this study, no clear relationship was observed between these two parameters, except for the fact that the maximum mean adsorption value was noted for the adsorbent with a mean pH_{eq} of 4.5, namely AF (Fig. S6, SI). This suggests that investigating adsorption based on artificially induced pH variations at equilibrium may be of limited relevance.

From a chemical point of view, both antibiotics and bioadsorbent components have functional groups that may undergo protonation/deprotonation, depending on the pH of the solution. This makes it possible for them to have positive, negative or neutral charges on the reactive surfaces, and thus facilitates the formation of various types of bonds.[45]

Additional details on the electrical charge of NAR, governed by its pK_a values[46–48] and determining its speciation under varying pH conditions, are provided in the SI.

As NAR has a pK_a (in water) of ~4.4,[48] within the pH_w values of 3.7 and 4.2 observed for PGP and PS, respectively, it is more soluble and exhibits positively charged functional groups (protonated), enabling it to engage in electrostatic interactions with the negatively charged surfaces of minerals and organic matter (OM) content.[49] All of this justifies their adsorption rates of 54.93% and 86.53%, respectively, recorded at 100 μmol L^{-1} of NAR.

At pH_w values above pK_a (>4.4), an increase in adsorption capacities was noted, since the antibiotic became less protonated and more negatively charged. This favored interactions with the positive charges of protonated amine groups ($-NH_3^+$) of the abundant OM present in all the investigated bioadsorbent, with values ranging between 17 and 68.4% (Table S3, SI).

In this case, the negatively charged NAR molecules tend to interact also with the negatively charged surfaces of bioadsorbents' organic matter, particularly the negative charges that appear in certain carboxylic acids ($-COO^-$) especially at pH_w levels above 5, *via* cationic bridge (especially using Na^+ and Ca^{2+}).[50,51]

This is in accordance with the fact that all the bioadsorbents contain carboxylic acids, with amounts ranging from 0.2 to 1.4 meq g^{-1} (Fig. S3, SI).

Alternatively, as the pH increases, the relative availability of cations in the equilibrium solution may also rise, thereby enhancing the likelihood of ionophores (such as NAR) transforming into neutral species. These neutral species could then be adsorbed by the organic phase, resulting in adsorption scores higher than those expected at lower pH levels.[24] However, considering adsorption results for the specific bioadsorbents under study, particularly CF and CGs (with pH_w values of 7.4 and 5.8, respectively), it can be remarked that adsorption rates recorded at the highest NAR concentrations (40–100 μmol L^{-1}). These concentrations are more environmentally relevant than the very low concentrations rarely detected in ecosystems, systematically decreased when pH_w exceeds 5.5, contradicting the typical trend observed for acidic chemicals beyond their pK_a values as a function of bioadsorbent pH.[24] These facts suggest that the sorption behavior of many pharmaceuticals in biomaterials cannot be predicted solely by pK_a values and/or solubility

factors, as other bioadsorbent characteristics, especially the OM contents, could influence the sorption process.[52]

As mentioned above, OM has variable charge, with negative charge raising as the pH increases, favoring higher NAR adsorption to these charged surfaces, probably *via* Ca^{2+} bridges, as NAR is mainly present in its neutral or anionic form at these pH_w levels ($pH_w \geq pK_a$). For this reason, PGP ($pH_w = 3.7$), even though it has a high content of OM (36.3%), as well as significant eCEC level (13.7 $cmol_c\ kg^{-1}$) (Table S3, SI), presents weaker adsorption capacity for NAR molecules. In some cases, bioadsorbents exhibiting lower OM content and eCEC levels show greater adsorption than PGP, as they have a $pH_w > 4.5$, resulting in a higher presence of negative charges, such as in PF and POF samples.

However, this is not a general trend, since higher OM content is typically associated with greater adsorption capacity for most bioadsorbents. This would explain the significant and positive correlations obtained between the removal rates noted at the maximum NAR concentration and the OM and organic carbon (OC%) contents ($r = 0.639$; $p < 0.01$) and the eCEC ($r = 0.378$; $p < 0.05$) (Table S4, SI). Owing to its potential to form complexes with monovalent and divalent cations (particularly Na^+ and Ca^{2+}), as is characteristic of ionophore antibiotics, adsorption scores recorded at highest NAR concentration were found to be positively and significantly correlated with Na_e ($r = 0.510$; $p < 0.05$) and Ca_e ($r = 0.665$; $p < 0.01$) contents present in the bioadsorbents. Moreover, the inverse effect of Mg_e content in bioadsorbent materials on their ability to retain ionophore antibiotics like MON has been previously reported[28] but was not detected in this study (Table S4, SI). However, a significant negative correlation with ash and volatile matter (VM) contents was found, exhibiting an $r = -0.478$ ($p < 0.05$), which aligns with the lower adsorption potential observed for the bioadsorbent with the highest ash content, notably CGs (Ash = 6.7%) (Tables S3 and S4, SI).

Other factors that showed a significative positive correlation and may favor the adsorption of NAR molecules onto the studied bioadsorbent include humidity and dry matter content ($r = 0.619$; $p < 0.01$), and porosity ($r = 0.416$; $p < 0.05$) (Tables S3 and S4, SI).

Notably, the substantial NAR adsorption observed in this study, particularly at concentrations of 40–100 μmol L^{-1}, for AB, EB, and AF (between 78.13–100%) (Fig. S4), aligns with previously reported MON retention by the same bioadsorbents (ranging 76.68–96.79%).[28] This suggests a broad affinity for ionophore molecules resulting from their ability to stablish both hydrophobic and polar interactions, as well as hydrogen bonding. Conversely, CF and PF, together with ZOB, exhibited weaker capacities to retain MON (between 10.17–46.11%) in comparison to NAR (34.92–84.92%) under identical antibiotic concentrations (40–100 μmol L^{-1}), indicating a preferential interaction with more hydrophobic compounds, possibly mediated by hydrophobic interactions and/or van der Waals forces. This pattern suggests that factors beyond hydrophobicity may also govern NAR binding to these materials.[28]

Additionally, Hussain and Prasher (2011)[24] reported pronounced NAR adsorption in soils at pH 6.8, influenced by OC% content and likely linked to its pK_a, which can reach 7.9 in organic solutions.

3.3 Influence of pH on the adsorption process

In the natural (unmodified) pH conditions, the percentage change in pH at the end of the experiment was marginal (3–4%) (Table S5, SI).

Studies involving pH change were conducted for the best adsorptive samples at 100 μmol L^{-1} of NAR (AF, EB, AB, AS, OP, and DPS) (Fig. S6, SI), which also exhibited the highest Al_o and Fe_o values (between 520–3010 mg kg^{-1} and 650–3265 mg kg^{-1}, respectively) (Table S3, SI).

The outcomes showed decreased sorption kinetics of all the six bioadsorbents analyzed at higher pH, which agrees with the trends reported elsewhere for monensin and lasalocid in soils.[43] This supports the assertion that, for many pharmaceuticals, adsorption behavior on bioadsorbents cannot be predicted solely from surrounding pH, but also depends on adsorbent properties. In this line, EB and AB, and to a lesser extent AF, exhibited the most stable adsorption across the entire pH range, maintaining efficiencies above 94.1%, 91.22%, and 82.3%, respectively, likely attributable to their high holocellulose content and abundant carboxylic acid groups (Table 1 and Fig. S3, SI). The EB sample proved particularly resilient, showing only ~6% loss across the full pH gradient. In contrast, OP, AS, and DPS displayed strong adsorption under acidic conditions but declined markedly at pH 10, indicative of weaker interactions under alkaline environments. These results highlight the critical role of surface chemistry in governing adsorption stability and suitability for different pH environments. Looking ahead, it would be possible to make additional changes in by-products with the lowest sorption capacities, for instance by coating them with Fe and/or Al oxides, as previously done on inert substrates such as quartz,[53] or through acid-activation processes.

3.4 Adapting the experimental data to different adsorption models

Fig. S7 (SI) shows the adsorption curves representing the experimental results obtained in this study for NAR and the set of the bioadsorbents tested. The curves plotting the experimental adsorption values (in μmol kg^{-1}) *versus* the equilibrium concentrations of NAR are of the S-type (not linear)[54] for most of the bioadsorbents, except for CF, PF, and CC, which exhibited concave (L-type) curves (Fig. S7, SI).

In S-type curves, adsorption percentage clearly increase with higher antibiotic concentrations, likely due to cooperative interactions between the antibiotic and the adsorbent, whereas the L-type pattern is indicative of the saturation of high-affinity adsorption sites, leading to a decline in adsorption efficiency (weaker interactions) at higher concentrations[42] (Fig. S7, SI). This explains why the samples having the S-type pattern are the most adsorptive ones, particularly at the highest concentrations tested (Fig. 1 and S7, SI). These shapes differ from those reported by Hamdi *et al.* (2024)[28] for MON sorption onto AB, EB, and AF, which displayed H-type curves (a special case of the L-

type pattern), whereas CF and PF also exhibited an L-type trend.[28]

In addition, Table 2 presents the values corresponding to the fitting of the experimental data to the Freundlich, Langmuir and Linear models for NAR and each of the bioadsorbents. Restricting the comments to those cases where error values associated with the fitting are not too high, comparing R^2 values it can be observed that the Freundlich model showed the best fit ($R^2 \geq 0.909$ for the 93% of the bioadsorbents), followed by the Langmuir model obtained $R^2 \geq 0.903$ for 36% of the materials, and the Linear model, with just 14% of the bioadsorbents exhibiting $R^2 \geq 0.956$ (Table 2). This means that the Freundlich model describes better the experimental data compared to the other two models, and that the sorption process is governed by surface heterogeneity and non-uniform energy distribution (in most cases).

Previous report[16] indicated that NAR sorption aligned well with the Freundlich equation in five soils with a relatively similar pH range (5.2–7.7), despite the bioadsorbents in the present study exhibiting higher OC% content (Table S3, SI). It is important to mention that the rather inadequate fit to the Langmuir model for 64% of the samples may be attributable to the fact that the thermodynamic saturation condition of the bioadsorbents was not reached as a sufficiently high concentration of the antibiotic was not added to achieve the saturation state.[55]

Also, the fact that the Linear model yields significantly lower R^2 values when predicting K_d parameter for most of the biosorbents (with a mean value of 0.757) indicates the absence of a linear relationship between the adsorption values and the initially added NAR concentrations.

The partition coefficient values (K_d) ranged between 15.96 and 212.58 L kg^{-1}, with the highest levels (101.87–212.58 L kg^{-1}) corresponding to the adsorption onto AF among fibers, AB and EB among barks, as well as OP, AS, and DPS from the agro-food by-products. All the latter samples are characterized by adsorption percentages close to 100% at the highest NAR concentration used (Fig. 1).

The highest K_d value (212.58 L kg^{-1}) was observed for AF, which may be related to its higher mean adsorption value (78.76%) with respect to the other bioadsorbents. In contrast, the remaining bioadsorbents showed lower K_d values, oscillating between 15.96 L kg^{-1} for CF and 81.57 L kg^{-1} for PS. In this case, the lowest K_d values noted for CF (15.96 L kg^{-1}) indicate greater NAR mobility in this sample, attributable to the weak affinity between the bioadsorbent particles and the adsorbate,[56] which matches the results of the adsorption percentage (Fig. 1 and S4).

Comparing these results with previous studies, lower K_d values were recorded for MON adsorption onto forest by-products (the same natural fibers and barks used here, except for the POF sample), ranging from 0.162 L kg^{-1} (ZOB) to 6.21 L kg^{-1} (CF),[28] as well as for SAL sorption onto raw and modified clays, with scores between 2.35–12.28 L kg^{-1}.[29]

As for the obtained K_F values, they confirm that AF within the fibers, both AB and EB among the barks, and AS, OP, and DPS from the agro-food by-products exhibit the highest affinity for NAR adsorption, with values between 754.15 and 923.45 L^n μmol^{1-n} kg^{-1}. Overall, the natural fibers, barks, and agro-food by-products displayed K_F mean values of 464.94, 744.31, and 536.6 L^n μmol^{1-n} kg^{-1}, respectively. Specifically, within the agro-food by-products, the stones and shells showed higher means (754.15 and 700.72 L^n μmol^{1-n} kg^{-1}, respectively) in comparison with those recorded for the peels and coffee-based adsorbents (519.79 and 280.52 L^n μmol^{1-n} kg^{-1}, respectively) (Table 2).

Given that the n values obtained are all >1, we can discard the presence of heterogeneous adsorption surfaces in these bioadsorbents.[57] Also, earlier studies indicated that $n > 1$ values are indicative of cooperative adsorption process, where previously sorbed molecules onto heterogeneous matrix enhance further sorption by modifying the surface.[58] In this work, the n values consistently range from 1.28 (CF) to 8.34 (EB), suggesting favorable conditions for non-linear and a heterogeneous adsorption,[59] and thus, a strong interaction between the adsorbents and adsorbate. In comparison, the natural barks

Table 2 Values of the NAR adsorption parameters for the Freundlich model (K_F and n), for the Langmuir model (K_L and q_m) and for the Linear model (K_d). R^2: coefficient of determination; E: error; —: error value too high for fitting

	Freundlich					Langmuir					Linear		
Sample	K_F (L^n μmol^{1-n} kg^{-1})	E	n	E	R^2	K_L (L Kg^{-1})	E	q_{max} (μmol kg^{-1})	E	R^2	K_d (L kg^{-1})	E	R^2
AF	923.45	73.39	8.12	1.49	0.937	0.45	0.05	1921.33	265.45	0.704	212.58	45.82	0.795
CF	130.67	86.12	1.28	0.15	0.881	—	—	994.58	231.72	0.851	15.96	4.367	0.784
PF	316	16.59	3.24	0.35	0.991	0.13	0.006	1229.73	455.26	0.981	44.68	13.82	0.965
POF	489.62	2.63	4.63	0.91	0.971	0.21	0.005	1551.84	355.41	0.897	63.57	26.15	0.897
AB	894.25	271.95	7.81	2.08	0.918	0.48	0.17	1971.9	501.49	0.723	159.37	37.55	0.593
EB	917.14	128.50	8.34	2.00	0.945	0.53	0.06	2003.56	636.44	0.856	173.92	44.61	0.657
ZOB	421.55	10.23	4.12	0.46	0.969	0.18	0.008	1478.45	197.15	0.676	56.87	21.94	0.586
OP	775.32	36.91	6.42	1.18	0.998	0.32	0.01	1862.71	456.73	0.967	116.94	37.84	0.896
PGP	264.26	1.49	2.42	0.14	0.983	0.09	0.007	1081.69	168.19	0.956	36.05	11.39	0.957
PS	558.42	17.87	5.44	0.53	0.965	0.26	0.027	1741.83	324.56	0.619	81.57	27.68	0.608
AS	843.03	127.85	6.73	1.82	0.973	0.38	0.078	1886.31	120.67	0.674	127.23	37.96	0.578
DPS	754.15	121.76	6.23	1.14	0.981	0.33	0.79	1814.82	235.89	0.645	101.87	31.54	0.653
CGs	228.63	1.16	2.03	0.13	0.971	0.07	0.08	1039.91	152.57	0.961	33.68	31.54	0.752
CC	332.42	41.75	3.78	0.16	0.909	0.15	0.018	1354.97	55.36	0.903	49.42	13.84	0.875

exhibit a higher mean value (6.75), while the fibers and agro-food by-products display relatively similar means of 4.31 and 4.72, respectively (Table 2). Specifically, AF (8.12), both AB and EB (7.81 and 8.34, respectively), OP, AS, as well as DPS (between 6.23–6.73) showed the highest n values, implying their greater adsorption capacity (Table 2), as confirmed by their higher removal rates relative to the other biomaterials. Comparatively, lower n values (ranging 0.21–2.68) were reported by Hamdi *et al.* (2024)[28] for MON in natural fibers and barks, with higher values recorded for EB, in aligns with the current findings.

Regarding the Langmuir equation, R^2 values exceeded 0.90 only for PF, the two peels (OP and PGP), and the coffee-based adsorbents (CGs and CC). This may suggest a coexistence of either multilayer adsorption (involving strong sorbent–sorbate interactions) or a monolayer system (characteristic of homogenous surfaces with a finite number of binding sites) adsorption, depending on the antibiotic concentration.

In this model, the q_{max} values generally oscillated between 994.58 (CF) and 2003.56 μmol kg^{-1} (EB), with the lowest values observed for CF, PGP, and CGs (Table 2), which agrees with their weaker affinities for adsorption. This is further supported by the corresponding K_L values, which ranged from 0.02 L kg^{-1} for CF and 0.53 L kg^{-1} for EB, with the lowest values found for the latter bioadsorbents.

It is important to emphasize that, considering the R^2 values, the Freundlich model is the only isotherm that could help in interpreting the NAR adsorption onto the studied by-products. Given that the higher the values of the K_F parameter, the stronger the adsorption capacity of the sorbent material, the relationships between the K_F values (along with n values) and the key characteristics of the biomaterials were examined (Table S6, SI), considering the whole set of sorbent by-products studied. The findings revealed that K_F values are positively and significantly correlated with several by-product parameters, including the OM and OC% contents ($r = 0.534$; $p < 0.05$), Na_e levels ($r = 0.741$; $p < 0.01$), porosity ($r = 0.584$; $p < 0.05$), humidity and dry matter content ($r = 0.703$; $p < 0.05$), and real and bulk density ($r = 0.625$ and $r = 0.562$, respectively; $p < 0.05$) (Table S6, SI). In contrast, negative and significative correlations were observed with only three parameters: exchangeable Mg_e ($r = -0.655$; $p < 0.05$) and ash and VM contents ($r = -0.830$; $p < 0.01$). The n values also exhibited a clear dependence on the same adsorbent characteristics, consistent with the K_F values but with somewhat smaller correlation coefficients (see r values in Table S6, SI).

Fig. S8 (SI) presents the Scatchard plots for all the bioadsorbents studied. The R^2 values obtained for the entire dataset were generally high (exceeding 0.811), except for CF, PGP, and CGs, which presented lower values (between 0.603–0.762). Specifically, the highest R^2 value was recorded for AF (0.987), consistent with its superior adsorption efficacy among the fourteen by-products, as reflected by a mean adsorption of 78.76%.

These outcomes are indicative of nonspecific or multiple interactions arising from the co-existence of diverse sorption sites on the by-product surfaces, thereby causing NAR molecules to exhibit either low (L) or high (H) affinities,[60] depending on both the antibiotic dose and the adsorbent type. Indeed, the Scatchard plots shown for CF, PF, and CC can be described as concave, reflecting a negative cooperative adsorption phenomenon and surface heterogeneity, in accordance with the observed decline in sorption capacity at higher NAR doses.[60] In contrast, the remaining bioadsorbents exhibited convex curves, characteristic of positive cooperative adsorption behavior.

Taken together with the above findings, this indicates that the primary factors governing NAR adsorption in this study were the type of adsorbent used and the initially added concentrations.

3.5 Adsorption mechanisms (FTIR and solid-state ^{13}C CP/MAS NMR analysis)

FTIR spectra of the bioadsorbents before (raw) and after NAR adsorption are shown in Fig. 2, with the wavenumbers listed in Tables S7a and S7b (SI). The detailed IR features (after NAR adsorption) are described in the SI, while this section focuses on discussing the influence of key functional groups, as reflected in the broader IR bands, on NAR adsorption.

Briefly, the stretch in the wide bands at 3292.69–3350 cm^{-1}, representing the O–H stretching vibrations of hydroxyl groups (H-donator sites), after NAR adsorption, indicating the establishment of successful hydrogen bonding (OH) interactions during adsorption (Fig. 2; Tables S7a and S7b, SI).

It is observed a significant stretching in the narrow peak at 2916–2985 cm^{-1}, characteristic of most agro-food bioadsorbents (except for CF and EB), along with their disappearance from the IR spectra of PF and their new emergence for EB spectra, which is indicative of the powerful combination of NAR molecules and the aliphatic C–H groups of these materials.[61] Conversely, these bands remain relatively stable in the IR spectra of fibers and barks (except for PF).

In parallel with the crucial role of lignin, reflected by the shifting of the wide peaks at 1726–1745 cm^{-1} for most bioadsorbents after NAR adsorption, except for PGP (see SI) where this peak disappears, the involvement of lignin components in strengthening interactions with the adsorbed molecules is further confirmed by the specific shift of the aromatic C=O stretches from 1600–1606 cm^{-1} to 1632–1636 cm^{-1}, observed in the typical IR spectra of PF and PS exposed to 100 μmol L^{-1} of NAR.[62]

Besides, following sorption, the increased intensity of peaks at 1026–1080 cm^{-1}, attributable to the C–O stretching vibration of carboxylic acids (cellulose),[63] for most bioadsorbents, along with the shifts of their wavenumbers to 1015–1018 cm^{-1} for barks and agro-food bioadsorbents (except for CGs and CC), may outline the formation of C–O bonds between NAR and the cellulosic fraction of the these bioadsorbents. This may also be reflected by the emergence of new peaks at 1097–1181.61 cm^{-1} range for OP and barks and their disappearance from the spectral profiles of fibers and all agro-food biosorbents after NAR adsorption (Fig. 2; Tables S7a and S7b, SI).

Notably, all peaks at wavenumbers ≤ 985 cm^{-1} indicate low concentrations of the corresponding groups or components, rendering them less relevant for NAR adsorption; nonetheless,

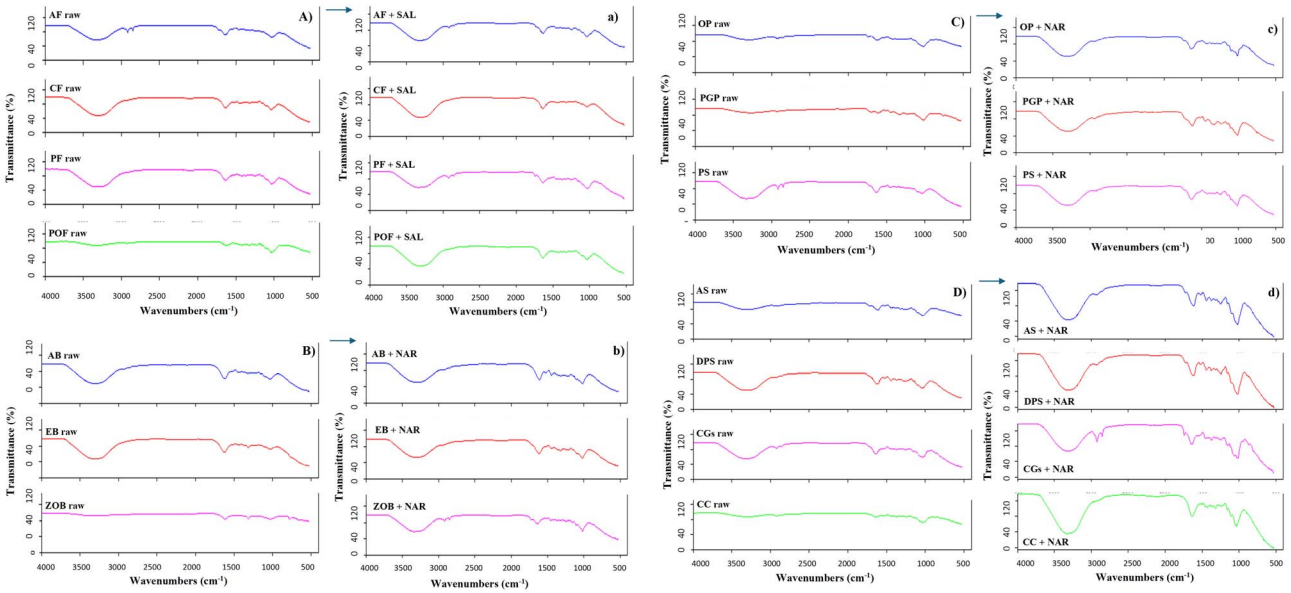

Fig. 2 FTIR spectra of all bio-adsorbents before (raw) and after NAR adsorption. (a) natural fibers; (b) natural barks; (c and d) agro-food by-products.

details on these peaks, along with the other preferential ones, are provided in the SI.

Overall, the non-significant changes in peaks identifying the presence of the antibiotic in the IR spectra of biomaterials with lower adsorption capacity at the highest NAR concentration (especially CF) could be attributed to (1) the lack of sensitivity of IR spectroscopy to proportionally small amounts of adsorbed antibiotic, and (2) the shielding effect of the bioadsorbent's porous structure on antibiotic signals. The functional groups present on the adsorbent surface were found to be essential factors governing the antibiotic–bioadsorbent interactions and influencing the efficiency of each bioadsorbent in removing the antibiotic, thus revealing the mechanisms involved in the adsorption process (Fig. 3).

This reasoning is further supported by the NMR spectra analysis, where results revealed comparatively higher content of O-alkyl C (between 57% for AF and AB and 66% for EB) and lower alkyl C (6–17%) signals on the NMR spectra of the most adsorptive by-products, as opposed to those recorded in the case biomaterials with the lowest adsorption capacity at 100 μmol L^{-1} of NAR (ZOB, PGP, and CGs, with values ranging between 40–47% and 8–26%, respectively) (Table S8 and Fig. S9, SI). These signals are most likely attributable to long chain aliphatic material and polysaccharides (primary cellulose and hemicellulose), respectively.[64] In relation to the adsorption process, elevated *O*-alkyl-C percentages together with comparatively low alkyl-C content promote hydrogen bonding and polar interactions (indicative of low hydrophobicity).

Furthermore, aromatic-C (15–29%) and carboxyl-C (5–11%) signals are markedly lower (Table S8, SI). It is known that aromatic-C corresponds lignin and tannin structures, whereas carboxyl C stands for carboxylic (COOH) and amide ($-CONH_2$)

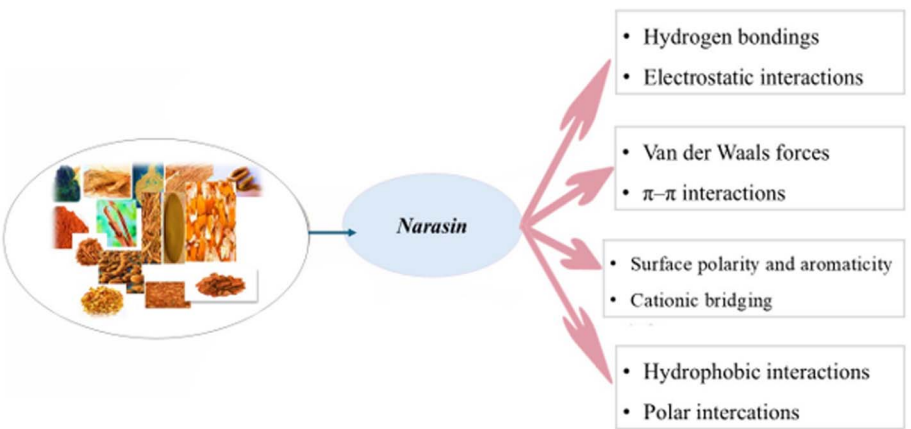

Fig. 3 Adsorption mechanisms of narasin onto the studied bio-adsorbents.

contributions.[64] A noteworthy observation is that aromatic-C rings did not stimulate NAR retention onto sorbent surfaces unless accompanied by low alkyl-C percentages and moderate carboxyl-C contents. This behavior is attributable to the diminished hydrophobic contribution of the aromatic moieties under such conditions, which constrains π–π interactions while rendering the polar sites less effective for binding, which is the case of ZOB, PGP, and especially CGs. In fact, it is become clear that both surface polarity and aromaticity act as dual and complementary contributors, governing the remarkable adsorption capacity of these biomaterials at the antibiotic doses used in this work. Additional details on NMR peak variations, highlighting comparative differences between the most and least adsorptive samples, are provided in the SI.

In summary, the FTIR spectra and solid-state ^{13}C CP/MAS NMR analysis identifies cellulose, hydroxyl, carbonyl, carboxyl, and amine groups as important functional groups responsible for adsorption in sorbent by-products. For future studies, scanning electron microscopy (SEM) micrographs could be acquired for the tested biomaterials, both before and after adsorption, to gain deeper insight into the structural properties responsible for adsorption and to elucidate the impact of the process on their morphological features.

3.6 Desorption of NAR and sorbent reusability

Fig. 4 depicts the NAR desorption from the investigated bioadsorbents, expressed as a percentage, *versus* the initially added concentrations (in μmol L^{-1}), whereas Fig. S10 (SI) presents the data in μmol kg^{-1}.

At the lowest NAR concentrations tested (5–20 μmol L^{-1}), desorption was generally below the detection limit for most bioadsorbents, except for those with higher pH_w levels (cactus fiber and the coffee-based bioadsorbents) (Fig. 4, Table S3, SI). Particularly, CF had the highest desorption at these three lowest concentrations, attaining 5.1% (40.8 μmol kg^{-1}) at 20 μmol L^{-1} of NAR (Fig. 4 and S10).

However, when the NAR concentration increased, the desorption rates rose as well, reaching 8.5% (166.52 μmol kg^{-1}), 10.4% (205.41 μmol kg^{-1}) and 14.6% (286.58 μmol kg^{-1}), at the 100 μmol L^{-1} dose of the antibiotic added for CGs, CC, and CF, respectively. This may be attributable to their higher pH_w levels compared to those observed for the other biomaterials studied. Similarly, for the remaining bioadsorbents, desorption continued to increase with higher concentrations, albeit remaining below 7% in all cases. Specifically, ZOB, as well as PF and POF samples, presented the highest desorption values, with scores of 6.2% (121.42 μmol kg^{-1}), 4.5% (88.02 μmol kg^{-1}), and 4.4% (86.06 μmol kg^{-1}), respectively, when the maximum concentration of NAR (100 μmol L^{-1}) was added (Fig. 4 and S10).

Generally, the most adsorptive by-products, at the highest three concentrations of NAR used (AF, both AB and EB, OP, AS, and DPS), showed desorption ranging from 0.5% (9.78 μmol kg^{-1}) to 1.62% (31.74 μmol kg^{-1}) (Fig. 4 and S10). This is in accordance with their richness in organic matter. Simultaneously, pomegranate peel and pea shell desorbed just 0.5% (9.78 μmol kg^{-1}) and 0.9% (17.60 μmol kg^{-1}), respectively at 100 μmol L^{-1} of NAR, which may be attributable to their lower pH_w values.

Fitting results listed in Table 3 indicated that the desorption experimental results were well-described by the Freundlich equation (with R^2 always ≥ 0.99) (Table 3). The $n_{(des)}$ values of this model deviated from unity for most of the tested by-products, assuming a non-linear relation between the concentration of narasin and its desorption from these biomaterials (Table 3). It was observed that adsorption was rather irreversible, with desorption $K_{d(des)}$ values consistently lower than those for adsorption, ranging from 6.67 to 21.42 L kg^{-1} (Table 3).

Globally, the $K_{d(des)}$ values for all the samples studied after desorption were notably higher than those obtained for MON desorption in agro-food by-products (0.03–0.7 L kg^{-1})[65] and in forest by-products (natural fibers and barks) (between 0.162–6.210 L kg^{-1}),[28] as well as for LAS desorption in fourteen agro-waste materials (1.23–26.78 L kg^{-1}).[66]

As indicated in Table S9 (SI), the average values of the hysteresis index (HI) are consistently in the range of 0.817–0.998 for all bioadsorbent samples (except CGs, with HI of 0.715), reflecting the slow desorption of the antibiotic.[67] Similar HI values were obtained by Hamdi *et al.* (2024)[28] for MON with the same natural adsorbent barks along with AF (always ≥ 0.906), meanwhile for CF and PF, lower average values (0.235 and 0.429, respectively) were detected. The acidic pH conditions can strengthen the interaction between adsorbate and the adsorbent surfaces by increasing the surface charge, which will reduce desorption percentages for NAR.[24] In this study, a decrease in desorption was observed for the adsorbents with lower pH_w levels (Fig. 4 and Table S3, SI). In fact, our outputs show that the desorption percentages recorded at the highest NAR concentration (100 μmol L^{-1}) are significantly and positively correlated with the pH levels (in water) when considering the data for all the bioadsorbents, with a correlation coefficient ($r = 0.634$, $p < 0.05$). On the contrary, no significant correlation was observed with the other physicochemical characteristics of the bioadsorbents.

Overall, the results confirm the strong NAR retention onto the studied biomaterials, causing that the adsorption process could be considered almost not reversible under the conditions of this research. These findings align with previous research proving greater NAR adsorption in sandy clay loam and sandy soils, with K_d values higher than those obtained for MON and SAL.[24]

To assess the reusability of the studied biomaterials, six successive regeneration cycles were performed on the by-products being those with the greatest adsorption efficacy at 100 μmol L^{-1} (above 60%), as the tests were conducted exclusively at this highest concentration (Fig. S11, SI). The results indicate that the 0.01 M HCl solution was not only effective in desorbing the antibiotic, but also in enhancing the surface characteristics of the adsorbents, thereby increasing the removal rates during cycles 1 and 2 for all the biomaterials tested (remaining close to 100%).

Notably, the most reusable by-products were EB and AB, whose adsorption never dropped below 95%, followed by AF

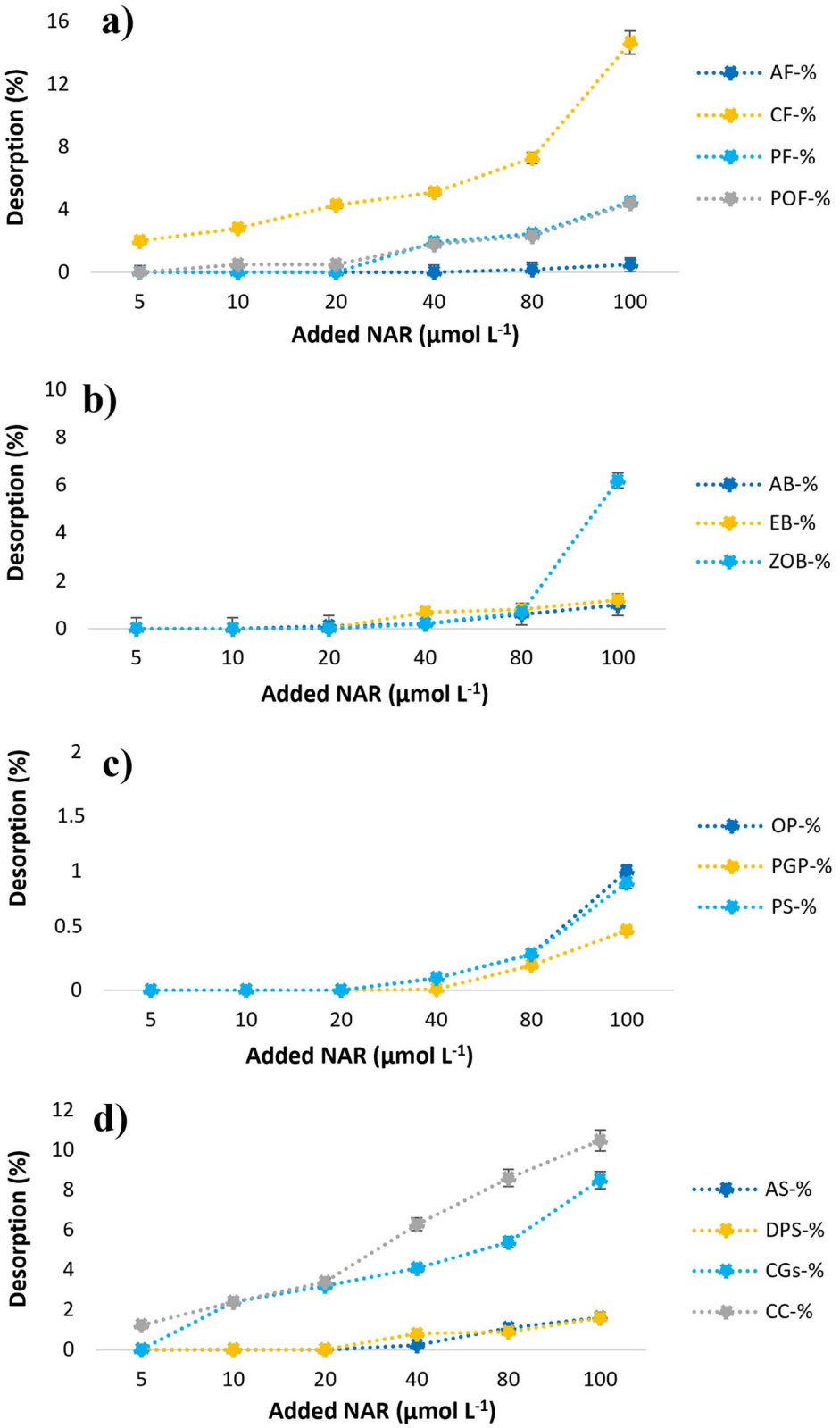

Fig. 4 Desorption curves of narasin (NAR) (expressed in µmol kg^{-1} and as %) from the natural fibers (a), barks (b), and the agro-food by-products (c and d), as a function of the antibiotic concentration added (µmol L^{-1}). Average values ($n = 3$), with coefficients of variation always <5%, and error bars represent the standard deviation.

Table 3 Values of the NAR desorption parameters for the Freundlich model (K_F and n), for the Langmuir model (K_L and q_m) and for the Linear model (K_d). R^2: coefficient of determination; E: error

	Freundlich					Langmuir					Linear		
Sample	K_F (L^n μmol^{1-n} kg^{-1})	E	n	E	R^2	K_L (L Kg^{-1})	E	q_{max} (μmol kg^{-1})	E	R^2	K_d (L kg^{-1})	E	R^2
AF	0.285	0.00	0 0.10	0.00	0.994	0.01	0.00	10.23	1.08	0.708	11.81	0.003	0.624
CF	28.14	4.23	0.84	0.14	0.996	0.45	0.011	292.09	21.34	0.779	6.67	0.007	0.714
PF	6.41	1.17	0.26	0.05	0.993	0.25	0.02	91.54	13.78	0.624	10.36	0.008	0.586
POF	23.09	1.03	0.75	0.03	1.00	0.37	0.04	89.34	16.33	0.689	19 0.82	3.44	0.543
AB	1.67	0.24	0.18	0.00	0.991	0.135	0.02	28.81	3.23	0.801	12.33	2.829	0.711
EB	1.71	0.12	0.19	0.001	0.998	0.18	0.015	26.47	0.54	0.742	11.58	0.160	0.6 92
ZOB	13.67	0.9	0.53	0.06	1.00	0.11	0.016	120.82	21.38	0.678	14.32	2.431	0.567
OP	0.797	0.00	0.23	0.19	0.993	0.24	0.00	27.83	1.37	0.760	21.42	0.069	0.6 62
PGP	2.19	0.06	0.16	0.062	0.996	0.16	0.04	14.72	0.69	0.762	11.26	0.043	0.7 05
PS	1.18	0.02	0.19	0.31	0.997	0.24	0.002	18.54	2.25	0.763	9.35	2.077	0.665
AS	0.86	0.07	0.31	0.17	0.999	0.16	0.00	32.04	5.92	0.768	15.78	1.135	0.566
DPS	0.154	0.02	0.34	5.57	0.994	0.19	0.024	35.51	7.63	0.670	20.53	0.366	0.521
CGs	15.71	4.06	0.60	2.35	0.995	0.78	0.001	178.92	10.189	0.802	13.45	0.666	0.712
CC	21.33	2.34	0.72	0.02	0.998	0.99	0.03	264.87	31.34	0.773	11.23	1.923	0.565

(≥93.23), with difference between cycle 1 and 2 around 3.8–6.17%. This trend may be attributable to their higher holocellulosic and carboxylic acid contents (63.52–75.1% and 1.2–1.4 meq g^{-1}, respectively), compared to OP, AS, and DPS (48.01–62.5% and 0.3–0.9 meq g^{-1}, respectively) (Table 1; Fig. S11, SI).

Conversely, the lowest regeneration ability was observed for OP sample, with a 17% decrease between cycles 1 and 6. In this context, orange peels have previously been used for the removal of heavy metals such as Cu(II) and Cd(II), displaying fluctuating performance and lower efficiency during repeated cycles. This is in accordance with their limited regeneration capacity against NAR molecules in the present study, which renders them unsuitable for repeated cycles of metal recovery.[68]

Although all the selected biomaterials (AF, AB, EB, OP, AS, and DPS) are cost-effective and readily available adsorbents with acceptable regeneration capacities, it should be emphasized that regenerating AS and OP required considerably more effort than the other samples, owing to their less rigid physical structure.

In contrast, AF and EB, due to their fibrous architecture, facilitated solvent penetration and faster desorption. Meanwhile, DPS, being dense and lignified (containing 30.2% of lignin and a bulk density of 1.3 g cm^{-3}), demonstrated satisfactory renderability (≥84.7%, with a difference of 11.5% between cycles 1 and cycle 2), appearing easier to regenerate than OP and AS.

In summary, the findings hold substantial significance for large-scale applications of these adsorbent biomaterials, particularly in wastewater depollution processes, given their wide availability and cost-effectiveness.

3.7 Economic assessment and environmental significance

The management of agricultural and forestry residues remains a noteworthy challenge, with the EU generating over 700 million tons of agricultural residues and 600 million tons of forestry by-products in 2020.[69,70] In North Africa, including Tunisia, agro-forest wastes such as fibers, fruit peels, shells, and coffee grounds are largely unexploited.[28,71] The disposal of these residues not only entails significant costs and environmental burden but also fails to provide economic return. Conversely, valorizing them as bioadsorbents for emerging pollutants, such as narasin, represents a cost-effective strategy for wastewater treatment. The feedstocks used in this study are inexpensive (≈15 € per ton) compared to conventional adsorbents (21.9–110 $ per ton),[72] which enhances their economic competitiveness. Regeneration of these adsorbents using hydrochloric acid (HCl) is more affordable and environmentally benign compared to supercritical extraction (SCE) methods, which require high-pressure devices. By-products exhibiting lower desorption, such as acacia and eucalyptus barks, efficiently reduce antibiotic concentrations in water and serve as sustainable alternatives to activated carbon. Altogether, this approach combines waste valorization, green processing, and efficient control of antibiotic contamination, thereby supporting both economic and environmental sustainability in agroforestry systems.

4 Conclusions

In this study, the adsorption–desorption behavior of different bioadsorbent by-products toward NAR was evaluated. Alfa fiber, acacia and eucalyptus barks, orange peel, almond shell, and date palm stones demonstrated a clearly greater adsorption capacity (≥74.46%) at NAR concentrations added above 20 μmol L^{-1}, likely due to their higher OM and carbon contents, as well as a cooperative adsorption mechanism (S-type curves). When the lowest concentrations are added (5–20 μmol L^{-1}), alfa, palm, and cactus fibers, as well as calcined coffee grounds show higher affinity (ranging 65.12–90%) for NAR, which then decreases as added concentration rises, indicating site saturation and a possible shift to lower-affinity binding. The best fit of the experimental data to the Freundlich model ($R^2 \geq 0.881$) suggests the predominance of multilayer adsorption on heterogenous surfaces. In addition, in this investigation, IR, NMR, and surface analyses provided a better understanding of the

functional groups and mechanisms involved in NAR adsorption onto the bioadsorbents. Concerning desorption, it remained below 10% for most bioadsorbents, even at high concentrations, except for calcined coffee grounds and cactus fiber (desorption reaching 10.48% and 14.64%, respectively, at 100 μmol L^{-1} of NAR added), indicating a strong adsorption of the antibiotic onto these bioadsorbents. Given that NAR desorption is low, the tested low-cost bioadsorbents could be considered in future studies as soil amendments to prevent NAR leaching from soils to surface water and groundwater. Overall, the current results are relevant in terms of controlling NAR pollution in water and other ecological matrices.

Conflicts of interest

There are no conflicts to declare.

Data availability

The data supporting this article have been included as part of the supplementary information (SI). Supplementary information is available. See DOI: https://doi.org/10.1039/d5ra09276k.

References

1 V. O. Stockwell and B. Duffy, Use of antibiotics in plant agriculture, *Rev. Sci. Tech. Off. Int. Epiz.*, 2012, **31**, 199–210, DOI: 10.20506/rst.31.1.2104.
2 S. W. Page and P. Gautier, Use of antimicrobial agents in livestock, *Rev. Sci. Tech. Off. Int. Epiz.*, 2012, **31**, 145–188, DOI: 10.20506/rst.31.1.2106.
3 S. Kuppusamy, D. Kakarla, K. Venkateswarlu, M. Megharaj, Y. E. Yoon and Y. B. Lee, Veterinary antibiotics (VAs) contamination as a global agro-ecological issue: A critical view, *Agric. Ecosyst. Environ.*, 2018, **257**, 47–59, DOI: 10.1016/j.agee.2018.01.026.
4 H. H. Azzaz, H. A. Murad and T. A. Morsy, Utility of ionophores for ruminant animals: A Review, *Asian J. Anim. Sci.*, 2015, **9**, 254–265, DOI: 10.3923/ajas.2015.254.265.
5 M. J. Rybicki, Coccidiostats in treating coccidiosis, *Żywność. Nauka. Technologia. Jakość*, 2020, **27**, 127–137, DOI: 10.15193/zntj/2020/125/364.
6 I. B. Ekinci, A. Chłodowska and M. Olejnik, Ionophore toxicity in animals: a review of clinical and molecular aspects, *Int. J. Mol. Sci.*, 2023, **24**, 16703, DOI: 10.3390/ijms24021696.
7 M. Hansen, K. A. Krogh, E. Björklund, A. Brandt and B. Halling-Sørensen, Environmental risk assessment of ionophores, *TrAC, Trends Anal. Chem.*, 2009, **28**, 534–542, DOI: 10.1016/j.trac.2009.02.015.
8 A. Wong, Unknown risk on the farm: Does agricultural use of ionophores contribute to the burden of antimicrobial resistance?, *mSphere*, 2019, **4**, 1–6, DOI: 10.1128/msphere.00433-19.
9 EFSA (European Food Safety Authority), Opinion of the scientific panel on contaminants in the food chain on a request from the European Commission on cross-contamination of non-target feeding stuffs by narasin authorised for use as a feed additive, *EFSA J.*, 2007, **552**, 1–35.
10 B. J. Kerr, S. L. Trabue, M. B. van Weelden, D. S. Andersen and L. M. Pepple, Impact of narasin on manure composition, microbial ecology, and gas emissions from finishing pigs fed either a corn-soybean meal or a corn-soybean meal-dried distillers grains with soluble diets, *J. Anim. Sci.*, 2018, **96**, 1317–1329, DOI: 10.1093/jas/sky053.
11 C. Hao, L. Lissemore, B. Nguyen, S. Kleywegt, P. Yang and K. Solomon, Determination of pharmaceuticals in environmental waters by liquid chromatography/electrospray ionization/tandem mass spectrometry, *Anal. Bioanal. Chem.*, 2006, **384**, 505–513, DOI: 10.1007/s00216-005-0199-y.
12 P. Sun, D. Barmaz, M. L. Cabrera, S. G. Pavlostathis and C. H. Huang, Detection and quantification of ionophore antibiotics in runoff, soil and poultry litter, *J. Chromatogr. A*, 2013, **1312**, 10–17, DOI: 10.1016/j.chroma.2013.08.044.
13 S. Sura, F. J. Larney, J. Charest, T. A. McAllister, J. V. Headley and A. J. Cessna, Veterinary antimicrobials in cattle feedlot environs and irrigation conveyances in a high-intensity agroecosystem in southern Alberta, Canada, *Environ. Sci. Pollut. Res.*, 2023, **30**, 12235–12256, DOI: 10.1007/s11356-022-22889-x.
14 P. Peippo, V. Hagren, T. Lövgren and M. Tuomola, Rapid time-resolved fluoroimmunoassay for the screening of narasin and salinomycin residues in poultry and eggs, *J. Agric. Food Chem.*, 2024, **52**, 1824–1828, DOI: 10.1021/jf030716o.
15 D. H. Berg and R. L. Hamill, The isolation and characterization of narasin, a new polyether antibiotic, *J. Antibiot.*, 1978, **31**, 1–6, DOI: 10.7164/antibiotics.31.1.
16 EFSA (European Food Safety Authority), Safety and efficacy of Monteban® G100 (narasin) for chickens for fattening, *EFSA J.*, 2018, **16**, 1–38, DOI: 10.2903/j.efsa.2018.5461.
17 S. C. Kim and K. Carlson, Occurrence of ionophore antibiotics in water and sediments of a mixed-landscape watershed, *Water Res.*, 2006, **40**, 2549–2560, DOI: 10.1016/j.watres.2006.04.036.
18 A. Barreiro, R. Cela-Dablanca, A. Míguez-González, D. Casagrande Pierantoni, C. Nebot, A. Núñez-Delgado, M. J. Fernández-Sanjurjo, and E. Álvarez-Rodríguez *Anticoccidia Presence in Slurries/manures and Agricultural Soils in Galicia (NW Spain)*, European Geosciences Union General Assembly, Vienna, Austria, 2024, vol. 14–19, DOI: 10.5194/egusphere-egu24-16991.
19 V. Furtula, E. G. Farrell, F. Diarrassoba, H. Rempel, J. Pritchard and M. S. Diarra, Veterinary pharmaceuticals and antibiotic resistance of Escherichia coli isolates in poultry litter from commercial farms and controlled feeding trials, *Poult. Sci.*, 2010, **29**, 180–188, DOI: 10.3382/ps.2009-00198.
20 S. L. DeVries, K. A. Block, M. Loving, L. Logozzo and P. Zhang, The effects of trace narasin on the biogeochemical N-cycle in a cultivated sandy loam, *Sci. Total Environ.*, 2020, **716**, 137031–137040, DOI: 10.1016/j.scitotenv.2020.137031.

21 T. Eggen, T. N. Asp, T. Grave and V. Hormazabal, Uptake and translocation of metformin, ciprofloxacin and narasin in forage- and crop plants, *Chemosphere*, 2011, **85**, 26–33, DOI: 10.1016/j.chemosphere.2011.06.041.

22 P. Herrero, F. Borrull, R. M. Marcé and E. Pocurull, Determination of polyether ionophores in urban sewage sludge by pressurised liquid extraction and liquid chromatography–tandem mass spectrometry: Study of different clean-up strategies, *J. Chromatogr. A*, 2013, **1285**, 31–39, DOI: 10.1016/j.chroma.2013.02.034.

23 A. Iglesias, C. Nebot, B. I. Vázquez, J. M. Miranda, C. M. Franco Abuín and A. Cepeda, Detection of veterinary drug residues in surface waters collected nearby farming areas in Galicia, North of Spain, *Environ. Sci. Pollut. Res.*, 2014, **21**, 2367–2377, DOI: 10.1007/s11356-013-2142-7.

24 S. A. Hussain and S. O. Prasher, Understanding the sorption of ionophoric pharmaceuticals in a treatment wetland, *Wetlands*, 2011, **31**, 563–571, DOI: 10.1007/s13157-011-0171-x.

25 A. Núñez-Delgado, E. Álvarez-Rodríguez, M. J. Fernández-Sanjurjo, J. C. Nóvoa-Muñoz, M. Arias-Estévez and D. Fernández-Calviño, Perspectives on the use of by-products to treat soil and water pollution, *Microporous Mesoporous Mater.*, 2015, **210**, 199–201, DOI: 10.1016/j.micromeso.2015.02.001.

26 B. Khiari, and M. Jeguirim Tunisian agro-food wastes recovery by pyrolysis: Thermogravimetric analysis and kinetic study, *10th International Renewable Energy Congress (IREC)*, Sousse, Tunisia, 2019, vol.978, pp. 1–5. DOI: 10.1109/IREC.2019.8754614.

27 A. Núñez-Delgado, Research on environmental aspects of retention/release of pollutants in soils and sorbents. What should be next?, *Environ. Res. J.*, 2024, **251**, 118593–118598, DOI: 10.1016/j.envres.2024.118593.

28 S. Hamdi, M. Issaoui, S. Hammami, A. Míguez-González, R. Cela-Dablanca, A. Barreiro, A. Núñez-Delgado, E. Álvarez-Rodríguez and M. J. Fernández-Sanjurjo, Removal of the highly toxic anticoccidial monensin using six different low-cost bio-Adsorbents, *Toxics*, 2024, **12**, 606–614, DOI: 10.3390/toxics12080606.

29 S. Hamdi, A. Míguez-González, R. Cela-Dablanca, A. Barreiro, M. J. Fernández-Sanjurjo, A. Núñez-Delgado and E. Álvarez-Rodríguez, Natural and modified clays as low-cost and ecofriendly materials to remove salinomycin from environmental compartments, *J. Environ. Manage.*, 2024, **368**, 122158–122176, DOI: 10.1016/j.jenvman.2024.122158.

30 N. Maaloul, P. Oulego, M. Rendueles, A. Ghorbal and M. Díaz, Novel biosorbents from almond shells: Characterization and adsorption properties modeling for Cu(II) ions from aqueous solutions, *J. Environ. Chem. Eng.*, 2017, **5**, 2944–2954, DOI: 10.1016/j.jece.2017.05.037.

31 M. A. Lopez-Velazquez, V. Santes, J. Balmaseda and E. Torres-Garcia, Pyrolysis of orange waste: a thermo-kinetic study, *J. Anal. Appl. Pyrolysis*, 2013, **99**, 170–177, DOI: 10.1016/j.jaap.2012.09.016.

32 K. Laloon, C. Junsiri, P. Sanchumpu and P. Ansuree, Factors affecting the biomass pellet using industrial eucalyptus bark residue, *Biomass Convers. Biorefin.*, 2022, **14**, 10101–10113, DOI: 10.1007/s13399-022-03126-4.

33 U. Michael-Igolima, S. J. Abbey, A. O. Ifelebuegu and E. U. Eyo, Modified orange peel waste as a sustainable material for adsorption of contaminants, *Materials*, 2023, **16**, 1092, DOI: 10.3390/ma16031092.

34 D. S. Rodrigues, P. O. Schmitt, L. A. Cordeiro, M. B. B. Rodrigues, A. C. R. Ribeiro, M. W. Bosenbecker, S. K. S. Silva, N. L. Carreno, D. A. Gatto, S. H. F. Silva, C. M. Cholant and A. L. Missio, Sustainable films derived from Eucalyptus spp. bark: Improving properties through chemical and physical pretreatments, *Polymers*, 2025, **17**, 1–105, DOI: 10.3390/polym17010105.

35 M. C. Ncibi, V. Jeanne-Rose, B. Mahjoub, C. Jean-Marius, J. Lambert, J. J. Ehrhardt, Y. Bercion, M. Seffen and S. Gaspard, Preparation and characterization of raw chars and physically activated carbons derived from marine Posidonia Oceanica (L.) fibers, *J. Hazard. Mater.*, 2009, **165**, 240–249, DOI: 10.1016/j.jhazmat.2008.09.126.

36 R. Khiari, M. F. Mhenni, M. N. Belgacem and E. Mauret, Chemical composition and pulping of date palm rachis and Posidona Oceanica-A comparison with other wood and non-wood fibre sources, *Bioresour. Technol.*, 2010, **101**, 775–780, DOI: 10.1016/j.biortech.2009.08.079.

37 M. Ayadi, C. Segovia, A. Baffoun, R. Zouari, V. Fierro, A. Celzard, S. Msahli and N. Brosse, Influence of anatomy, microstructure, and composition of natural fibers on the performance of thermal insulation panels, *ACS Omega*, 2023, **8**, 48673–48688, DOI: 10.1021/acsomega.3c02481.

38 M. Fiserova, J. Gigac, A. N. Majtnerova and G. A. Szeiffova, Evaluation of annual plants (Amaranthus caudatus L., Atriplex hortensis L., Helianthus tuberosus L.) for pulp production, *Cellul. Chem. Technol.*, 2006, **40**, 405, DOI: 10.5772/intechopen.92112.

39 O. A. Fakayode and K. E. Abobi, Optimization of oil and pectin extraction from orange (Citrus sinensis) peels: a response surface approach, *J. Anal. Sci. Technol.*, 2018, **9**, 20–32, DOI: 10.1186/s40543-018-0151-3.

40 S. Ben-Ali, Application of raw and modified pomegranate peel for wastewater treatment: a Literature overview and analysis, *Int. J. Chem. Eng.*, 2021, **19**, 8840907, DOI: 10.1155/2021/8840907.

41 A. Dąbrowski, Adsorption-from Theory to Practice, *Adv. Colloid Interface Sci.*, 2001, **93**, 135–224, DOI: 10.1016/S0001-8686(00)00082-8.

42 P. Sipos, Searching for optimum adsorption curve for metal sorption on soils: comparison of various isotherm models fitted by different error functions, *SN Appl. Sci.*, 2021, **3**, 387–400, DOI: 10.1007/s42452-021-04383-0.

43 S. A. Sassman and L. S. Lee, Sorption and degradation in soils of veterinary ionophore antibiotics: monensin and lasalocid, *Environ. Chem.*, 2007, **26**, 1621, DOI: 10.1897/07-073R.1.

44 R. A. Figueroa-Diva, D. Vasudevan and A. A. MacKay, Trends in soil sorption coefficients within common antimicrobial

families, *Chemosphere*, 2010, **79**, 786–793, DOI: 10.1016/j.chemosphere.2010.03.017.

45 H. Sun, X. Shi, J. Mao and D. Zhu, Tetracycline sorption to coal and soil humic acids: An examination of humic structural heterogeneity, *Environ. Toxicol. Chem.*, 2010, **29**, 1934–1942, DOI: 10.1002/etc.248.

46 Chemical Book. *Narasin 55134-13-9-Chemical Book*. Retrieved March 10, 2025, from https://www.chemicalbook.com/ChemicalProductProperty_EN_CB3756283.htm.

47 S. A. Hussain, S. O. Prasher and R. M. Patel, Removal of ionophoric antibiotics in free water surface constructed wetlands, *Ecol. Eng.*, 2012, **41**, 13–21, DOI: 10.1016/j.ecoleng.2011.12.006.

48 S. A. Bak, M. Hansen, K. A. Krogh, A. Brandt, B. Halling-Sørensen and E. Björklund, Development and validation of an SPE methodology combined with LC-MS/MS for the determination of four ionophores in aqueous environmental matrices, *Int. J. Environ. Anal. Chem.*, 2013, **93**, 1500–1512, DOI: 10.1080/03067319.2013.763250.

49 H. Chen, L. Q. Ma, B. Gao and C. Gu, Effects of Cu and Ca cations and Fe/Al coating on ciprofloxacin sorption onto sand media, *J. Hazard. Mater.*, 2013, **252–253**, 375–381, DOI: 10.1016/j.jhazmat.2013.03.014.

50 T. Martinek, F. G. Riddell and C. F. Wilson, The conformations of narasin–metal complexes in solution determined by NMR spectroscopy, *J. Chem. Soc.*, 2000, **2**, 2192–2198, DOI: 10.1039/b005618i.

51 M. E. Parolo, M. J. Avena, G. R. Pettinari and M. T. Baschini, Influence of Ca^{2+} on tetracycline adsorption on montmorillonite, *J. Colloid Interface Sci.*, 2012, **368**, 420–426, DOI: 10.1016/j.jcis.2011.10.079.

52 K. L. Chen, L. C. Liu and W. R. Chen, Adsorption of sulfamethoxazole and sulfapyridine antibiotics in high organic content soils, *Environ. Pollut.*, 2017, **231**, 1163–1171, DOI: 10.1016/j.envpol.2017.08.011.

53 M. Pateiro-Moure, A. Bermúdez-Couso, D. Fernández-Calviño, M. Arias-Estévez, R. Rial-Otero and J. Simal-Gándara, Paraquat and Diquat sorption on iron oxide coated quartz particles and the effect of phosphates, *J. Chem. Eng. Data*, 2010, **55**, 2668–2672, DOI: 10.1021/je900945h.

54 C. H. Giles, D. Smith and A. Huitson, A general treatment and classification of the solute adsorption isotherm. I, Theoretical, *J. Colloid Interface Sci.*, 1974, **47**, 755–765, DOI: 10.1016/0021-9797(74)90252-5.

55 H. N. Tran, S. N. You and H. P. Chao, Thermodynamic parameters of cadmium adsorption onto orange peel calculated from various methods: A comparison study, *J. Environ. Chem. Eng.*, 2016, **4**, 2671–2682, DOI: 10.1016/j.jece.2016.05.009.

56 J. C. Deng, X. Jiang, X. Lü, G. F. Yu, F. Wang and B. Zhang, Atrazine adsorption behavior on a fluvo-aquic soil as influenced by contact periods, *Pedosphere*, 2007, **17**, 786–791, DOI: 10.1016/S10020160(07)60094-0.

57 K. Y. Foo and B. H. Hameed, Insights into the modeling of adsorption isotherm systems, *Chem. Eng. J.*, 2010, **156**, 2–10, DOI: 10.1016/j.cej.2009.09.013.

58 W. Kong, C. Li, J. M. Dolhi, S. Li, J. Z. He and M. Qiao, Characteristics of oxytetracycline sorption and potential bioavailability in soils with various physical-chemical properties, *Chemosphere*, 2012, **87**, 542–548, DOI: 10.1016/j.chemosphere.2011.12.062.

59 M. Mohapatra, K. Rout, B. Mohapatra and S. Anand, Sorption behavior of Pb(II) and Cd(II) on iron ore slime and characterization of metal ion loaded sorbent, *J. Hazard. Mater.*, 2009, **166**, 1506–1513, DOI: 10.1016/j.jhazmat.2008.12.081.

60 M. E. Roca Jalil, M. Baschini and K. Sapag, Removal of ciprofloxacin from aqueous solutions using pillared clays, *Materials*, 2017, **10**, 1345, DOI: 10.3390/ma10121345.

61 K. Ferchichi, N. Amdouni, Y. Chevalier and S. Hbaieb, Low-cost Posidonia oceanica bio-adsorbent for efficient removal of antibiotic oxytetracycline from water, *Environ. Sci. Pollut. Res.*, 2022, **29**, 83112–83125, DOI: 10.1007/s11356-022-21647-3.

62 S. Cataldo, A. Gianguzza, D. Milea, N. Muratore, A. Pettignano and S. Sammartano, A critical approach to the toxic metal ion removal by hazelnut and almond shells, *Environ. Sci. Pollut. Res.*, 2018, **25**, 4238–4253, DOI: 10.1007/s11356-017-0779-3.

63 M. El Achaby, N. Fayoud, M. C. Figueroa-Espinoza, H. Ben Youcef and A. Aboulkas, New highly hydrated cellulose microfibrils with a tendril helical morphology extracted from agro-waste material: application to removal of dyes from wastewater, *RSC Adv.*, 2018, **8**, 5212–5224, DOI: 10.1039/c7ra10239a.

64 X. Wang, R. Cook, S. Tao and B. Xing, Sorption of organic contaminants by biopolymers: role of polarity, structure and domain spatial arrangement, *Chemosphere*, 2007, **66**, 1476–1484, DOI: 10.1016/j.chemosphere.2006.09.004.

65 S. Hamdi, M. Issaoui, S. Hammami, A. Míguez-González, R. Cela-Dablanca, A. Barreiro, A. Núñez-Delgado, E. Álvarez-Rodríguez and M. J. Fernández-Sanjurjo, Repurposing agro-food wastes to remove monensin from the environment. Euro-M editerr, *J. Environ. Integr.*, 2025, **11**, 3, DOI: 10.1007/s41207-025-00979-9.

66 S. Hamdi, M. Issaoui, S. Hammami, A. Míguez-González, R. Cela-Dablanca, A. Barreiro, A. Núñez-Delgado, E. Álvarez-Rodríguez and M. J. Fernández-Sanjurjo, Agro-waste materials: a low-cost approach to emerging contaminant mitigation, *Bioresour. Technol. Rep.*, 2025, **32**, 10241, DOI: 10.1016/j.biteb.2025.102412.

67 Y. Li, T. Pan, D. Miao, Z. Chen and Y. Tao, Sorption-desorption of typical tetracyclines on different soils: environment hazards analysis with partition coefficients and hysteresis index, *Environ. Eng. Sci.*, 2015, **32**, 19–335, DOI: 10.1089/ees.2014.0325.

68 A. A. Bhran, S. Tadepalli, K. S. R. Murthy and A. A. AlGhamdi, Biosorption and regeneration studies for Cu (II) and Cd (II) removal from industrial effluents using orange peel and

composite adsorbents, *Processes*, 2025, **13**, 1972, DOI: 10.3390/pr13071972.

69 N. Scarlat, F. Fahl, E. Lugato, F. Monforti-Ferrario and J. F. Dallemand, Integrated and spatially explicit assessment of sustainable crop residues potential in Europe, *Biomass Bioenergy*, 2019, **122**, 257–269, DOI: 10.1016/j.biombioe.2019.01.021.

70 FAO, *Statistics on forestry production and trade (FOASTAT-Forestry)*, 2020, available at: http://www.fao.org/faostat.

71 A. Singh, R. Dikshit and N. Singh, Valorization of agro-industrial wastes for biorefinery products, *Waste Biomass Valorization*, 2023, **14**, 1–20, DOI: 10.1007/s12649-022-01687-2.

72 M. A. Ahmed, J. L. Zhou, H. H. Ngo and W. Guo, Insight into biochar properties and its cost analysis, *Biomass Bioenergy*, 2016, **84**, 76–86, DOI: 10.1016/j.biombioe.2015.11.002.